


# Synthesis of $\text{TiO}_2/\text{SiO}_2/\text{Ag}/\text{Ag}_2\text{O}$ and $\text{TiO}_2/\text{Ag}/\text{Ag}_2\text{O}$ nanocomposite spheres with photocatalytic performance

Anquan Deng<sup>1,2</sup> · Yufu Zhu<sup>1</sup> 

Received: 21 November 2017 / Accepted: 1 March 2018 / Published online: 10 March 2018  
© Springer Science+Business Media B.V., part of Springer Nature 2018

**Abstract**  $\text{TiO}_2/\text{SiO}_2/\text{Ag}/\text{Ag}_2\text{O}$  and  $\text{TiO}_2/\text{Ag}/\text{Ag}_2\text{O}$  nanocomposite spheres have been synthesized via a low-temperature hydrothermal method using  $\text{SiO}_2$  spheres as templates, combined with a light-induced reduction method and a hydrogen peroxide oxidation process. Scanning electron microscopy, energy-dispersive X-ray and X-ray diffraction analyses have demonstrated that Ag and  $\text{Ag}_2\text{O}$  nanoparticles were successfully deposited on the surfaces of  $\text{TiO}_2/\text{SiO}_2$  nanocomposite spheres and porous  $\text{TiO}_2$  nanospheres forming nanoheterojunctions. The photocatalytic experiment results reveal that all the as-prepared catalysts possess improved photocatalytic activities compared with P25 nanoparticles. Both  $\text{TiO}_2/\text{SiO}_2/\text{Ag}/\text{Ag}_2\text{O}$  and  $\text{TiO}_2/\text{Ag}/\text{Ag}_2\text{O}$  nanocomposite spheres exhibit excellent photocatalytic performances, which can be attributed to the synergistic effects of different kinds of nanoparticles. The synergistic mechanism of these nanoparticles is also discussed in detail.

**Keywords**  $\text{TiO}_2/\text{SiO}_2/\text{Ag}/\text{Ag}_2\text{O}$  · Nanocomposite spheres · Nanoheterojunction · Photocatalytic activities

---

✉ Yufu Zhu  
hyit2014@163.com

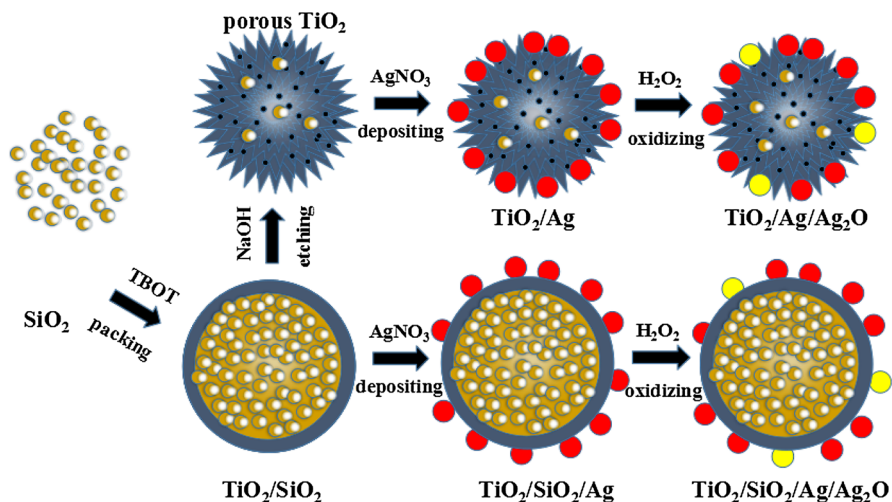
<sup>1</sup> Faculty of Mechanical and Material Engineering, Huaiyin Institute of Technology, Huaian 223003, People's Republic of China

<sup>2</sup> College of Material Science and Engineering, Nanjing Tech University, Nanjing 21009, People's Republic of China

## Introduction

Nowadays, with the constant deterioration of the global ecological environment, it is urgently required to synthesize an economical and non-polluting material that can effectively degrade a variety of harmful organic pollutants in sewage [1–3]. The application of semiconductor nanomaterials in the field of photocatalysis has attracted widespread concern. For example,  $\text{TiO}_2$  [4],  $\text{WO}_3$  [5],  $\text{SiO}_2$  [6],  $\text{Ag}_2\text{O}$  [7] and  $\text{ZnO}$  [8] have been widely used as photocatalysts. Among them, nano- $\text{TiO}_2$  is the most widely studied semiconductor photocatalyst because of its outstanding photo-induced activity and lack of secondary pollution [2, 9, 10]. Previous researches have proved that the photocatalytic ability of  $\text{TiO}_2$  strongly depends on its morphology and size [11–13]. For instance, porous nano-sized  $\text{TiO}_2$  and  $\text{TiO}_2$  nanorods generally have better photocatalytic performance than commercial P25 nanoparticles (NPs), owing to their larger surface area and more reactive sites [14, 15]. Unfortunately, there are some drawbacks that hinder the application of  $\text{TiO}_2$  catalysts due to the limitations of the material properties, such as large energy gap, high photoelectron–hole recombination rate and so on [16, 17]. Hence, researchers are seeking more effective ways to increase the surface active sites, photoelectron–hole separation rates, solar energy utilization efficiency and spectral responses for enhancing the photocatalytic properties of  $\text{TiO}_2$  [18–20].

Related reports demonstrate that both the noble metals (e.g., Ag, Au, Cu) and semiconductors (e.g.,  $\text{Ag}_2\text{O}$ ,  $\text{CuO}$ ,  $\text{Cu}_2\text{O}$ ) coupled with  $\text{TiO}_2$  photocatalysts can expand spectral responses and reduce photoelectron–hole recombination rates of  $\text{TiO}_2$  [21–24]. Ag NPs deposited on the surface of semiconductors (such as  $\text{TiO}_2$ ) can involve the surface plasmon resonance (SPR) effect. In particular, the Ag NPs, acting as a photoelectron catcher, have been widely applied because of their excellent performance in degrading water-borne organic pollutants compared with other noble metals [1]. Moreover, the band gap energy (1.46 eV) of p-type  $\text{Ag}_2\text{O}$  semiconductors is lower than that of  $\text{TiO}_2$  [25]. A *p-n* nanoheterojunction consisting of *p*-type  $\text{Ag}_2\text{O}$  and *n*-type  $\text{TiO}_2$  will lead to a lower photoelectron–hole recombination rate and wider spectral response; therefore, it has enhanced photocatalytic properties [26]. On the other hand, it has been reported that nano- $\text{SiO}_2$  possesses high stability, good adsorption, large specific surface and multiple surface active sites, and are usually used as the carrier or core of various composite materials [18, 27, 28]. Consequently,  $\text{TiO}_2/\text{SiO}_2$  core/shell nanostructures should have a larger specific surface area, higher thermal stability, better dispersion properties and more adsorption sites than pure  $\text{TiO}_2$  NPs. This also confirms that  $\text{TiO}_2/\text{SiO}_2$  core/shell nanostructures show superior photocatalytic activity [29–31]. In recent years,  $\text{TiO}_2$  doped with  $\text{Cu}_2\text{O}/\text{Cu}$  [32], B/N [33], Ag/ $\text{Ag}_2\text{O}$  [34],  $\text{SiO}_2/\text{Fe}_3\text{O}_4$  [35] and  $\text{Fe}_3\text{O}_4/\text{SiO}_2/\text{Ag}$  [36] have been synthesized and used as photocatalysts. A few studies have found that  $\text{TiO}_2/\text{Ag}/\text{Ag}_2\text{O}$  nanocomposites exhibit superior photocatalytic activity compared with pure  $\text{TiO}_2$  due to the combined action of Ag and  $\text{Ag}_2\text{O}$  NPs [34, 37–39]. However, there have been very few studies on the photocatalytic ability of  $\text{TiO}_2/\text{SiO}_2/\text{Ag}/\text{Ag}_2\text{O}$  nanocomposite structures.



**Scheme 1** The synthesis process of the  $\text{TiO}_2/\text{Ag}/\text{Ag}_2\text{O}$  and  $\text{TiO}_2/\text{SiO}_2/\text{Ag}/\text{Ag}_2\text{O}$  nanocomposite spheres

In the current work, as shown in Scheme 1,  $\text{TiO}_2/\text{SiO}_2$  nanocomposite spheres were first prepared by a hydrothermal method at low temperature using seeded silica spheres as templates and tetrabutyl titanate (TBOT) as the titanium source, and then  $\text{TiO}_2/\text{SiO}_2$  nanocomposite spheres were etched by sodium hydroxide solution to obtain porous  $\text{TiO}_2$  nanospheres. Subsequently, Ag NPs were immobilized on the synthesized catalysts through a light-induced reduction method, and then partially oxidized by hydrogen peroxide to synthesize  $\text{TiO}_2/\text{SiO}_2/\text{Ag}/\text{Ag}_2\text{O}$  and  $\text{TiO}_2/\text{Ag}/\text{Ag}_2\text{O}$  nanocomposite spheres. The photocatalytic performances of the as-prepared photocatalysts were evaluated by the photodegradation of RhB solution under simulated solar irradiation. The results show that  $\text{TiO}_2/\text{SiO}_2/\text{Ag}/\text{Ag}_2\text{O}$  and  $\text{TiO}_2/\text{Ag}/\text{Ag}_2\text{O}$  nanocomposite spheres have highly efficient photocatalytic abilities.

## Experimental

### Chemicals

All chemical reagents were of analytical grade and used without further purification. Ammonia solution ( $\text{NH}_3 \cdot \text{H}_2\text{O}$ , 35.05%), sodium hydroxide (NaOH, 96%), silver nitrate ( $\text{AgNO}_3$ , 99.8%) and absolute ethanol were obtained from Sinopharm Chemical Reagent (China). TBOT ( $\text{Ti}(\text{OC}_4\text{H}_9)_4$ , 99%), acetonitrile ( $\text{C}_2\text{H}_3\text{N}$ , 99%), silica sphere (50 nm), hydrogen peroxide ( $\text{H}_2\text{O}_2$ , 30%), ammonium oxalate ( $(\text{NH}_4)_2\text{C}_2\text{O}_4$ , 99.8%), sodium sulfate ( $\text{NaSO}_4$ , 99%), isopropanol ( $\text{C}_3\text{H}_8\text{O}$ , 99.5%) and titanium tetrachloride ( $\text{TiCl}_4$ , 99%) were obtained from Shanghai Aladdin Bio-Chem Technology (China). The commercial P25 was obtained from Degussa (Germany).

## Preparation of seeded silica templates

In order to facilitate crystal growth, the silica templates were pretreated with titanium tetrachloride ( $\text{TiCl}_4$ ) solution. The detailed experimental procedures are as follows. First, the silica templates were calcined at 500 °C for 30 min. Then, 1 g of the sintered silica templates was dispersed in 8 mL of 0.3 mM  $\text{TiCl}_4$  aqueous solution and maintained in a sealed container at 70 °C for 1 h. The treated silica templates were collected by centrifugation and washed with deionized water. The dried seeded templates were calcinated at 500 °C for 30 min. The above steps were repeated three times.

## Synthesis of $\text{TiO}_2/\text{SiO}_2$ nanocomposite spheres

$\text{TiO}_2/\text{SiO}_2$  nanocomposite spheres were prepared via a hydrothermal method using the pre-treated silica spheres as templates. First, 15 mL of absolute ethanol and 0.3 mL of deionized water were well mixed with 5 mL of acetonitrile, followed by adding 0.1 g of the seeded silica templates to the above mixed solution under ultrasound irradiation. Then, 60  $\mu\text{L}$  of  $\text{NH}_3\cdot\text{H}_2\text{O}$  was added to the suspension under magnetic stirring. After 30 min, 1.6 mL of TBOT was added and stirred for 15 min. Finally, the sealed Teflon-lined autoclave containing the mixed solution was heated at 120 °C for 3 h. The obtained  $\text{TiO}_2/\text{SiO}_2$  nanocomposite spheres were washed using deionized water and absolute ethanol, dried, and calcined at 400 °C for 3 h. By controlling the hydrothermal reaction conditions, a series of  $\text{TiO}_2/\text{SiO}_2$  nanocomposite spheres were obtained.

## Synthesis of porous $\text{TiO}_2$ nanospheres

First, a series of  $\text{TiO}_2/\text{SiO}_2$  nanocomposite spheres were obtained by the following hydrothermal conditions: 1.3 mL TBOT for 3 h, 1.6 mL TBOT for 3 h and 1.6 mL TBOT for 8 h, which were denoted as S0, S1 and S2, respectively. Then, these catalysts were collected and thoroughly washed with deionized water. The wet samples were then immersed in 2 M NaOH aqueous solution at 80 °C for 1 h. Finally, the silica cores were removed to obtain porous  $\text{TiO}_2$  nanospheres. The obtained catalysts were washed and calcined at 400 °C for 3 h. The final porous nanospheres were denoted as PSN-0, PSN-1 and PSN-2, respectively.

## Synthesis of $\text{TiO}_2/\text{Ag}$ nanocomposite spheres

The  $\text{TiO}_2/\text{Ag}$  nanocomposite spheres were synthesized according to a previously reported method [1]. First, 25 mg of the obtained porous  $\text{TiO}_2$  nanospheres (PSN-1) were added into 15 mL of absolute ethanol containing 15 mg of  $\text{AgNO}_3$ . The suspension was ultrasonically treated for 10 min and then stirred for 1 h under a 300-W Xenon lamp irradiation. The dark purple powder was collected and dried in a vacuum environment at 50 °C. The dried  $\text{TiO}_2/\text{Ag}$  nanocomposite spheres were calcined at 400 °C for 3 h.

## Synthesis of TiO<sub>2</sub>/Ag/Ag<sub>2</sub>O nanocomposite spheres

The TiO<sub>2</sub>/Ag/Ag<sub>2</sub>O nanocomposite spheres were fabricated by partially oxidization of silver nanoparticles with hydrogen peroxide on the surface of TiO<sub>2</sub>/Ag nanocomposite spheres [40]. Then, 5 mg of TiO<sub>2</sub>/Ag nanocomposite spheres were well dispersed in 20 mL of deionized water, and 2.22 mL of H<sub>2</sub>O<sub>2</sub> was slowly dripped into the solution and then stirred for 2 h at room temperature. A light yellow powder was obtained and was washed with deionized water and absolute ethanol. The final catalysts were calcined at 400 °C for 3 h to obtain TiO<sub>2</sub>/Ag/Ag<sub>2</sub>O nanocomposite spheres. The synthesis of the TiO<sub>2</sub>/SiO<sub>2</sub>/Ag/Ag<sub>2</sub>O nanocomposite spheres can also be obtained using the same preparation process as described above.

## Synthesis of TiO<sub>2</sub>/Ag<sub>2</sub>O nanocomposite spheres

The synthesis of TiO<sub>2</sub>/Ag<sub>2</sub>O nanocomposite spheres was conducted through a modified method of that described in Ref. [41]. First, 0.1 g of porous TiO<sub>2</sub> nanospheres (PSN-1) was uniformly dispersed in 25 mL of deionized water. Then, 0.213 g of AgNO<sub>3</sub> was added to the suspension and 0.1 M NaOH aqueous solution was added until the pH of the mixture was around 12–13. Next, the mixture was stirring constantly for 30 min at room temperature. Finally, the TiO<sub>2</sub>/Ag<sub>2</sub>O nanocomposite spheres were obtained under UV irradiation for 10 min. The final catalysts were calcined at 400 °C for 3 h.

## Catalyst characterization

The morphologies of the as-prepared catalysts were characterized by a field emission scanning electron microscope (FE-SEM; Quanta 250 FEG; FEI) and transmission electron microscopy (TEM; JEM-2100F; JEOL). Energy dispersive spectroscopy (EDS) analysis of the catalysts was carried out using an energy dispersive spectrometer (INCA-Max 20; Oxford). The crystal structures of the catalysts were studied with an X-Ray diffractometer (XRD; D8 AVANCE; Bruker). The energy band gap of the catalysts was determined from UV–Vis DRS spectrum in the 200–600 nm range, recorded by a UV–Vis spectrophotometer (UV-3600; Shimadzu).

## Photocatalytic measurement

The photocatalytic performance of the prepared catalysts was assessed via the degradation of Rhodamine B (RhB) in aqueous solution under simulated solar irradiation. During the experiment, H<sub>2</sub>O<sub>2</sub> solution was added to enhance the separation rate of the photoelectron–hole and photocatalytic properties. In a typical experimental process, 0.0075 g of the catalyst and 0.3 mL of 30% of H<sub>2</sub>O<sub>2</sub> were added to 30 mL of RhB aqueous solution (25 mg L<sup>-1</sup>). Prior to the photocatalytic degradation, the suspended liquid was first sonicated for 5 min, and then stirred constantly in the dark for 1 h. A Xenon lamp (300 W, PLS-SXE300C) was used as the simulated solar light source in the photocatalytic experiments. The distance

between the lamp and photoreactor was 13 cm. All the catalytic experiments were carried out at a fixed light intensity. The suspension was irradiated at set intervals under simulated solar light. Several milliliter liquids were taken out and the catalysts were removed by centrifugation. The obtained supernatant concentration was finally examined between the wavelength of 400 and 700 nm by the UV–Vis spectrophotometer. The trapping experiments of the active species were carried out according to the above steps, except for adding  $\text{H}_2\text{O}_2$ . Ammonium oxalate (3 mg), sodium sulfate (3 mg) and isopropanol (3  $\mu\text{L}$ ), used as hole ( $\text{h}^+$ ), electron ( $\text{e}^-$ ) and OH radicals ( $\text{OH}^\cdot$ ) scavengers, were added to above reaction solution, respectively.

## Results and discussion

### Characterization of $\text{TiO}_2/\text{SiO}_2$ nanocomposite spheres

The morphologies and structures of the obtained catalysts were studied by SEM analysis. Figure 1 shows the SEM images of the  $\text{TiO}_2/\text{SiO}_2$  nanocomposite spheres at different magnifications prepared with silica spheres as templates. From the SEM image shown in Fig. 1a, it can be seen that the surface of the silica spheres was packed with a layer of  $\text{TiO}_2$  film after the hydrothermal reaction with 1.6 mL TBOT for 3 h. The high-magnification SEM images shown in Fig. 1b clearly demonstrate that the synthesized  $\text{TiO}_2/\text{SiO}_2$  nanocomposite spheres have a peculiar and rough

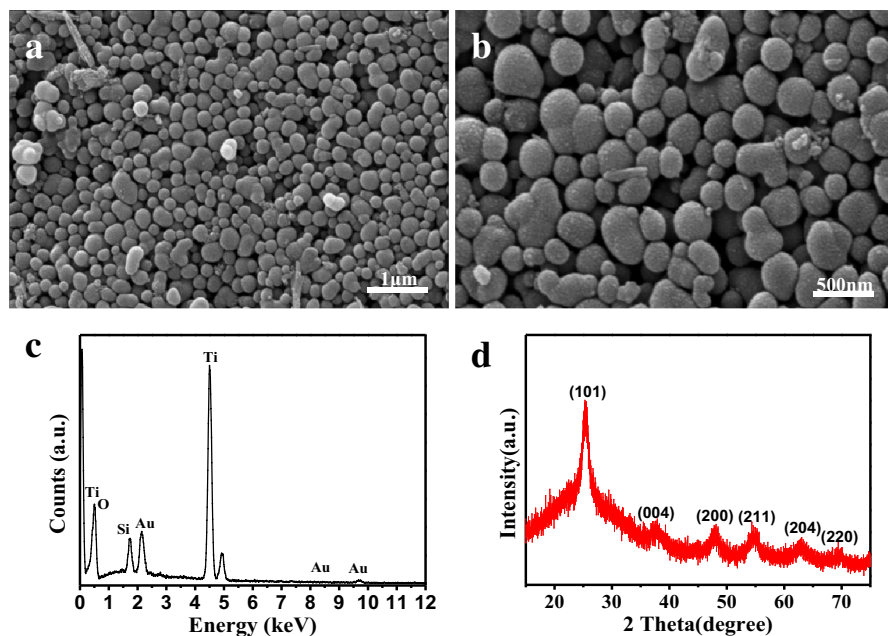


**Fig. 1** a, b SEM images, c EDS spectrum and d XRD pattern of  $\text{TiO}_2/\text{SiO}_2$  nanocomposite spheres obtained by hydrothermal reaction with 1.6 mL TBOT for 3 h

surface with an average diameter of about 400 nm. The reason for the formation of this peculiar morphology may be because of the exposure of a part of the silica core. The results of the energy spectrum analysis (EDS) and phase analysis (XRD) also strongly show the above results, as shown in Fig. 1c, d. The typical EDS spectrum in Fig. 1c shows that the prepared catalysts contain the following three elements: O, Ti and Si, which indicates that the presence of the Si element in the obtained TiO<sub>2</sub>/SiO<sub>2</sub> nanocomposite spheres. The results of XRD characterization indicate that the obtained TiO<sub>2</sub>/SiO<sub>2</sub> nanocomposite spheres are composed of anatase crystallite (JCPDS. 21-1272) [42] (Fig. 1d). The wide diffraction peak at about 25.3° may originate from the amorphous silica templates embedded in the obtained products.

### Characterization of porous TiO<sub>2</sub> nanospheres

By adjusting the hydrothermal reaction conditions, a series of TiO<sub>2</sub>/SiO<sub>2</sub> nanocomposite spheres were obtained. The synthesis of porous TiO<sub>2</sub> nanospheres with different morphologies (PSN-0, PSN-1 and PSN-2) was realized by etching the nanocomposites in sodium hydroxide aqueous solution, as shown in Fig. 2. From the SEM images shown in Fig. 2a, b, one can see that the surface of PSN-0 was partially etched by sodium hydroxide solution. The average diameter of the porous TiO<sub>2</sub> nanospheres is approximately 300 nm. With increasing the amount of TBOT, the thickness of the titania layer deposited on the surface of silica is increased. Eventually, the pores in the surface of TiO<sub>2</sub> nanospheres will be more clearly exposed after sodium hydroxide etching, as shown in Fig. 2c, d. With increasing the hydrothermal reaction time to 8 h, the average diameter of the porous TiO<sub>2</sub> nanospheres was slightly increased. As demonstrated in Fig. 2e, f, a small agglomeration and lower porosity exposure can be found due to the increased thickness of the titania layer.

EDS and XRD analysis were used to confirm the elemental and phase compositions of porous TiO<sub>2</sub> nanospheres formed after sodium hydroxide etching. Figure 2g shows the EDS spectrum of the as-prepared PSN-1, which indicates that the elemental compositions of the porous TiO<sub>2</sub> nanospheres are O, Ti and Si. At the same time, it can be observed that the peak corresponding to the Si element decreases substantially compared with that demonstrated in Fig. 1c. Therefore, the above EDS results indicate that the obtained porous TiO<sub>2</sub> nanospheres contain a small amount of residual silica. The X-ray diffraction patterns of PSN-1 are shown in Fig. 2h, from which it can be seen that the characteristic peaks at 25.4°, 48.0° and 62.6° can be indexed to the (101), (200), (211) and (204) planes of anatase TiO<sub>2</sub> (JCPDS. 21-1272), respectively. Moreover, the characteristic peak at about 25.3° is similar to that of the TiO<sub>2</sub>/SiO<sub>2</sub> nanocomposite spheres. This further proves that porous nanospheres are composed of anatase TiO<sub>2</sub> and amorphous SiO<sub>2</sub>.

### Characterization of TiO<sub>2</sub>/Ag, TiO<sub>2</sub>/Ag/Ag<sub>2</sub>O and TiO<sub>2</sub>/Ag<sub>2</sub>O nanocomposite spheres

Porous TiO<sub>2</sub>/Ag, TiO<sub>2</sub>/Ag/Ag<sub>2</sub>O and TiO<sub>2</sub>/Ag<sub>2</sub>O nanocomposite spheres were synthesized in order to investigate their photocatalytic properties. To systematically

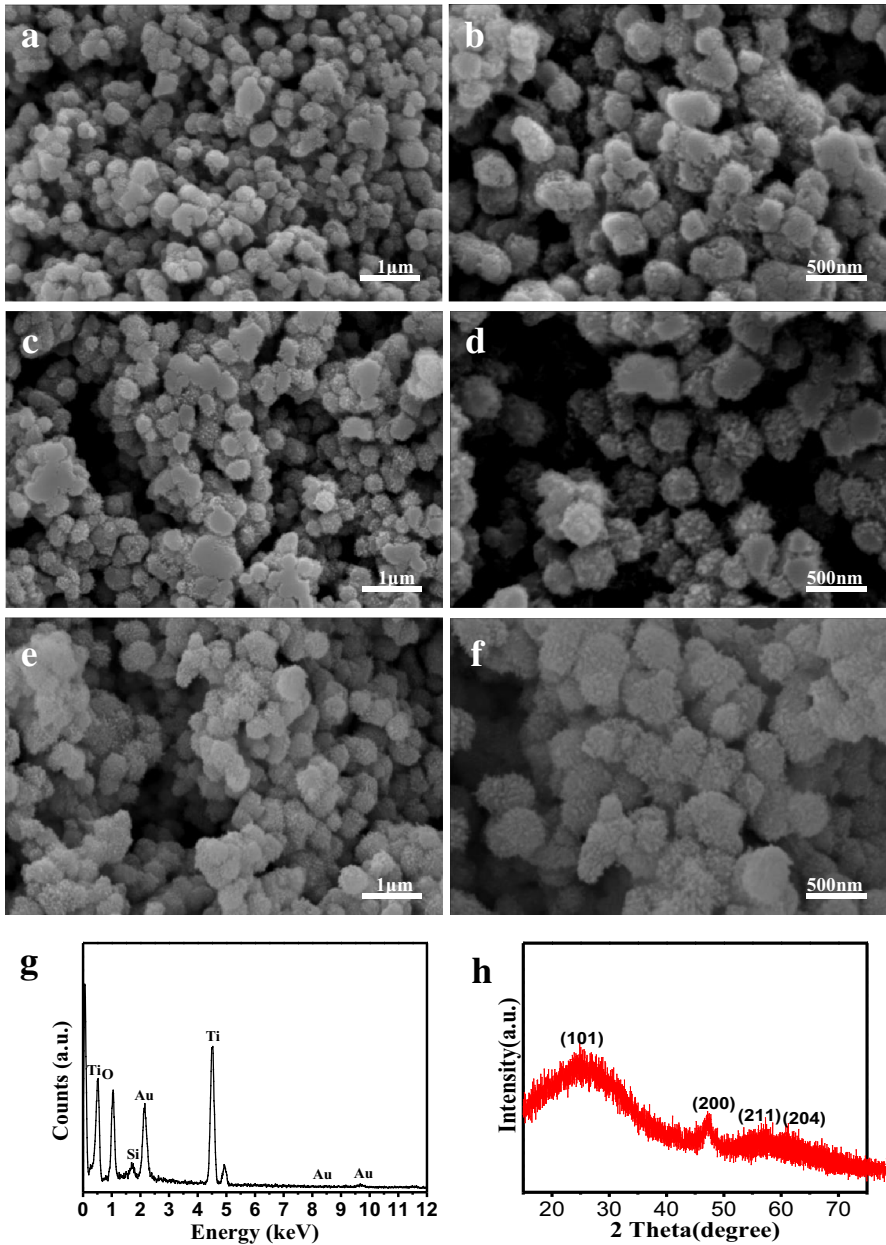


**Fig. 2** SEM images of porous TiO<sub>2</sub> nanospheres catalysts **a, b** PSN-0, **c, d** PSN-1, **e, f** PSN-2. EDS spectrum (**g**) and XRD pattern (**h**) of porous TiO<sub>2</sub> nanospheres

compare the surface morphology and further verify the composition of the obtained porous TiO<sub>2</sub> nanocomposite spheres, SEM and EDS analyses were performed. The SEM image of TiO<sub>2</sub>/Ag nanocomposite spheres is presented in Fig. 3a. It can be



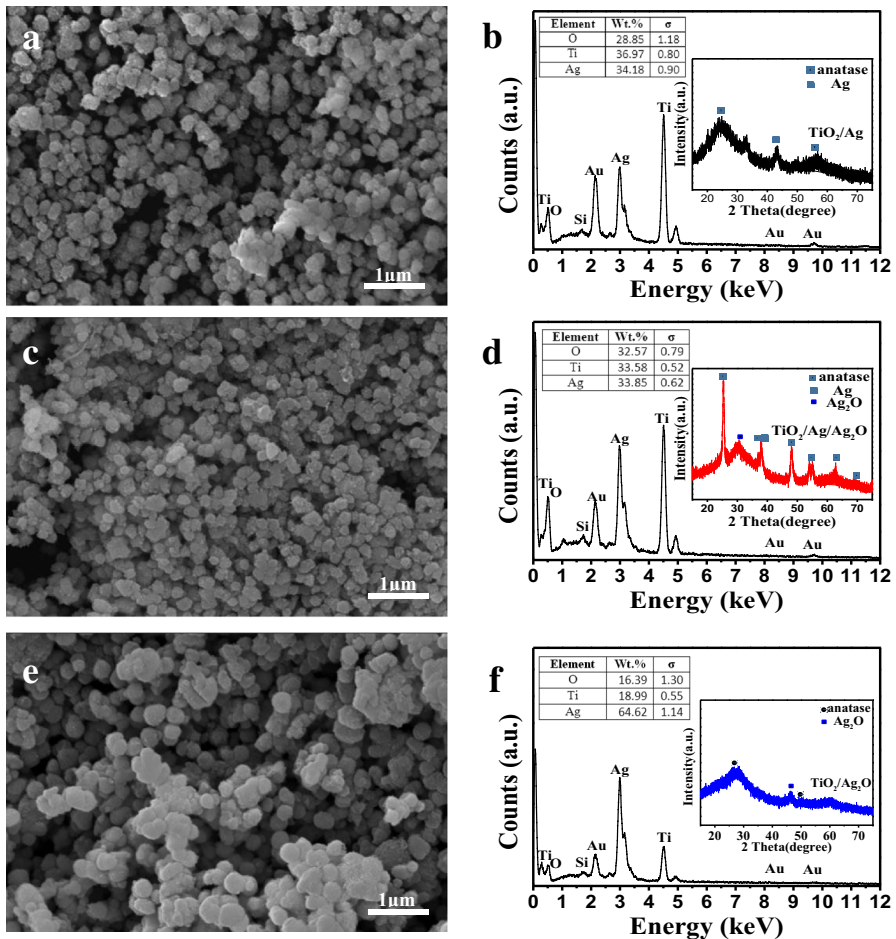


**Fig. 3** SEM images, EDS spectrums and XRD patterns of the catalysts: **a, b** TiO<sub>2</sub>/Ag, **c, d** TiO<sub>2</sub>/Ag/Ag<sub>2</sub>O and **e, f** TiO<sub>2</sub>/Ag<sub>2</sub>O

distinctly seen that the diameter of nanocomposite spheres did not change very much compared to the SEM results of porous TiO<sub>2</sub> nanospheres. The EDS spectrum shown in Fig. 3b demonstrates that the weight percents of O, Ti and Ag in the obtained catalysts are 28.85, 36.97 and 34.18%, respectively. In addition, there is a very weak characteristic peak of Si, which indicates that the obtained catalyst may contain a small amount of silica nanoparticles. In order to further clarify the crystal structure of the TiO<sub>2</sub>/Ag nanocomposite spheres, the typical XRD pattern is displayed in the inset of Fig. 3b. In addition to the characteristic peaks of anatase TiO<sub>2</sub>, a peak centered at  $2\theta = 44.58^\circ$  appears, which corresponds to the (200) plane of Ag (JCPDS. 03-0921) [43]. The above analysis confirms the presence of Ag in the obtained nanocomposite spheres. After partially oxidizing with hydrogen peroxide solution, although the surface morphology of the catalysts shows no obvious change, its composition ratio has changed, as displayed in Fig. 3c, d. From

the interpolation table in Fig. 3d, one can see that the weight percent of the O element increases from 28.85 to 32.57%, while that of the Ti and Ag elements all decrease slightly. This may be caused by the partial oxidation of Ag in the catalyst. As displayed in the inset of Fig. 3d, the overall contour of the XRD patterns of  $\text{TiO}_2/\text{Ag}/\text{Ag}_2\text{O}$  nanocomposite spheres is similar to anatase  $\text{TiO}_2$ , except for the peak of Ag and  $\text{Ag}_2\text{O}$  (JCPDS. 41-1104) [44], indicating the existence of Ag and  $\text{Ag}_2\text{O}$  in the nanocomposite spheres. Therefore, it seems rational to draw a conclusion that the Ag immobilized on the porous  $\text{TiO}_2$  nanospheres was partially oxidized to form  $\text{TiO}_2/\text{Ag}/\text{Ag}_2\text{O}$  nanocomposite spheres. Figure 3e, f shows the SEM image and EDS spectrum of  $\text{TiO}_2/\text{Ag}_2\text{O}$  nanocomposite spheres. From the XRD pattern shown in the inset of Fig. 3f, in addition to the characteristic peaks of anatase  $\text{TiO}_2$ , a weak diffraction peak at  $46.14^\circ$  can be observed [45]. This suggests that  $\text{Ag}_2\text{O}$  was successfully formed on the surface of the porous  $\text{TiO}_2$  nanospheres. It is noted that the synthesized  $\text{TiO}_2/\text{Ag}$ ,  $\text{TiO}_2/\text{Ag}/\text{Ag}_2\text{O}$  and  $\text{TiO}_2/\text{Ag}_2\text{O}$  nanocomposite spheres contain a small amount of  $\text{SiO}_2$  due to the incomplete etching of the  $\text{SiO}_2$  embedded in the spherical structures, as demonstrated in Scheme 1.

### Characterization of $\text{TiO}_2/\text{SiO}_2/\text{Ag}/\text{Ag}_2\text{O}$ nanocomposite spheres

For a more systematic comparison,  $\text{TiO}_2/\text{SiO}_2/\text{Ag}/\text{Ag}_2\text{O}$  nanocomposite spheres were fabricated via the same preparation method as the  $\text{TiO}_2/\text{Ag}/\text{Ag}_2\text{O}$  nanocomposite spheres. Figure 4a, b shows the SEM images of the fabricated catalysts with low and high magnifications. Compared with the  $\text{TiO}_2/\text{SiO}_2$  nanocomposite spheres, no morphological changes were observed. TEM analysis of the nanocomposite spheres was also carried out and the results are shown in Fig. 4c, d. It can be seen from Fig. 4d that Ag and  $\text{Ag}_2\text{O}$  NPs were effectively fabricated on  $\text{TiO}_2$  by the light-induced reduction method and the hydrogen peroxide oxidation process.

As exhibited in Fig. 4e, the EDS spectrum indicates the existence of four elements (O, Si, Ti and Ag) in the nanocomposite spheres. Moreover, the XRD analysis was performed to determine the crystal structure of the spheres. The result of the XRD analysis is shown in Fig. 4f. Compared with the XRD pattern shown in Fig. 1d, it is apparent that several weak diffraction peaks corresponding to Ag and  $\text{Ag}_2\text{O}$  can be seen, which indicates the formation of  $\text{TiO}_2/\text{SiO}_2/\text{Ag}/\text{Ag}_2\text{O}$  nanocomposite spheres.

### UV–Vis DRS analysis

Figure 5a shows the UV–Vis diffuse reflectance spectra of the obtained catalysts, from which one can see that several nanocomposite catalysts exhibit higher adsorption in the visible region compared with porous  $\text{TiO}_2$  nanospheres, especially  $\text{TiO}_2/\text{Ag}$ ,  $\text{TiO}_2/\text{Ag}/\text{Ag}_2\text{O}$  and  $\text{TiO}_2/\text{Ag}/\text{Ag}_2\text{O}$  nanocomposite spheres. This indicates that the formation of various nanoparticles on  $\text{TiO}_2$  surfaces can bring about a change in the spectral response of catalysts. By using the Kubelka–Munk equation  $[(F(R_\infty)/hv)^{1/2}]$  vs.  $hv$  (photo energy), the estimated energy band gap ( $E_g$ ) of catalysts can be obtained. As shown in Fig. 5b, the estimated  $E_g$  value of the porous

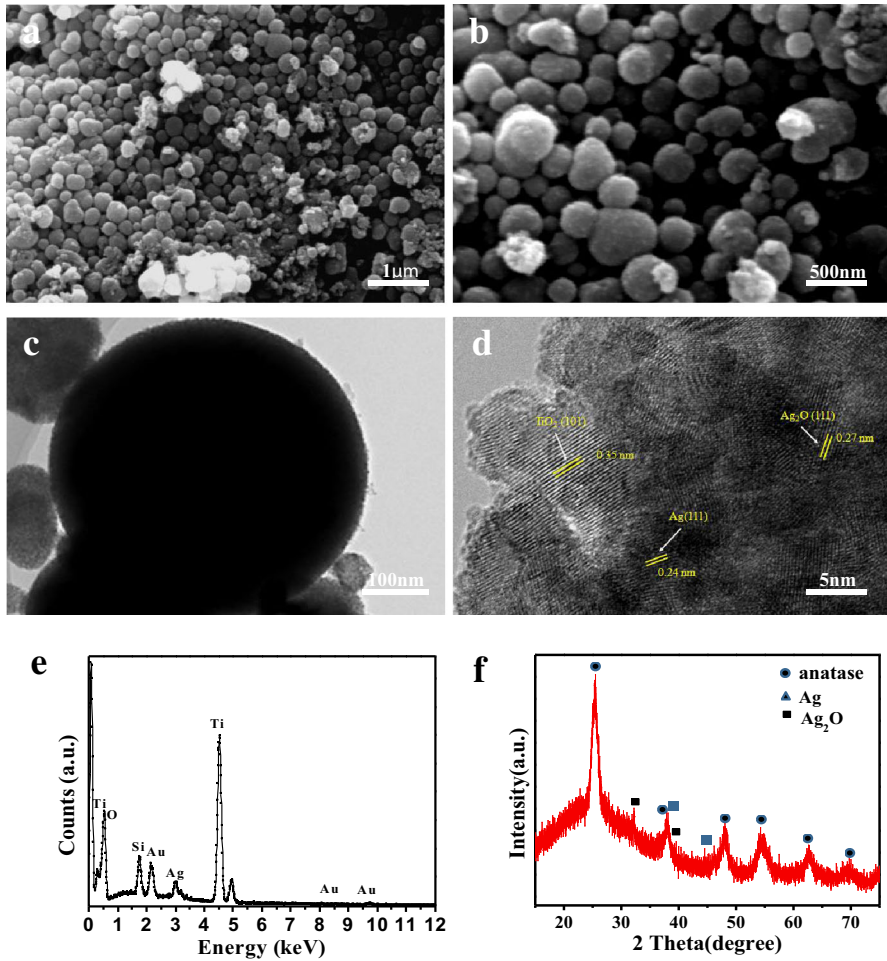


**Fig. 4** SEM images (a, b), TEM image (c), HRTEM image (d), EDS spectrum (e) and XRD pattern (f) of TiO<sub>2</sub>/SiO<sub>2</sub>/Ag/Ag<sub>2</sub>O nanocomposite spheres

TiO<sub>2</sub> nanospheres is 3.20 eV, which is consistent with the reported energy band gap of anatase TiO<sub>2</sub> ( $E_g = 3.0\text{--}3.2$  eV). With the introduction of Ag, Ag<sub>2</sub>O and SiO<sub>2</sub> nanoparticles, the  $E_g$  values of nanocomposite catalysts decrease to values in the range of 2.19–3.01 eV.

### Photocatalytic measurement

To study the effect of catalyst composition and its structure on photocatalytic performance, the photo-degradation experiments of RhB were conducted under simulated solar irradiation. During the experimental process, the photocatalytic properties of TiO<sub>2</sub>/SiO<sub>2</sub>, TiO<sub>2</sub>, TiO<sub>2</sub>/Ag, TiO<sub>2</sub>/Ag<sub>2</sub>O, TiO<sub>2</sub>/Ag/Ag<sub>2</sub>O and TiO<sub>2</sub>/SiO<sub>2</sub>/Ag/Ag<sub>2</sub>O were investigated. The photocatalytic performance of commercial

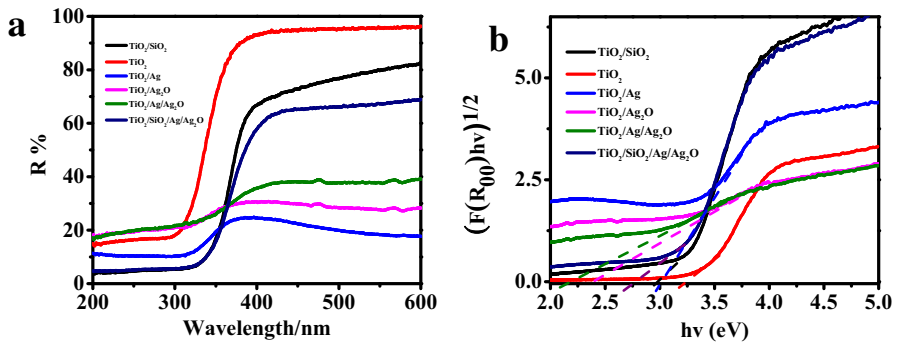
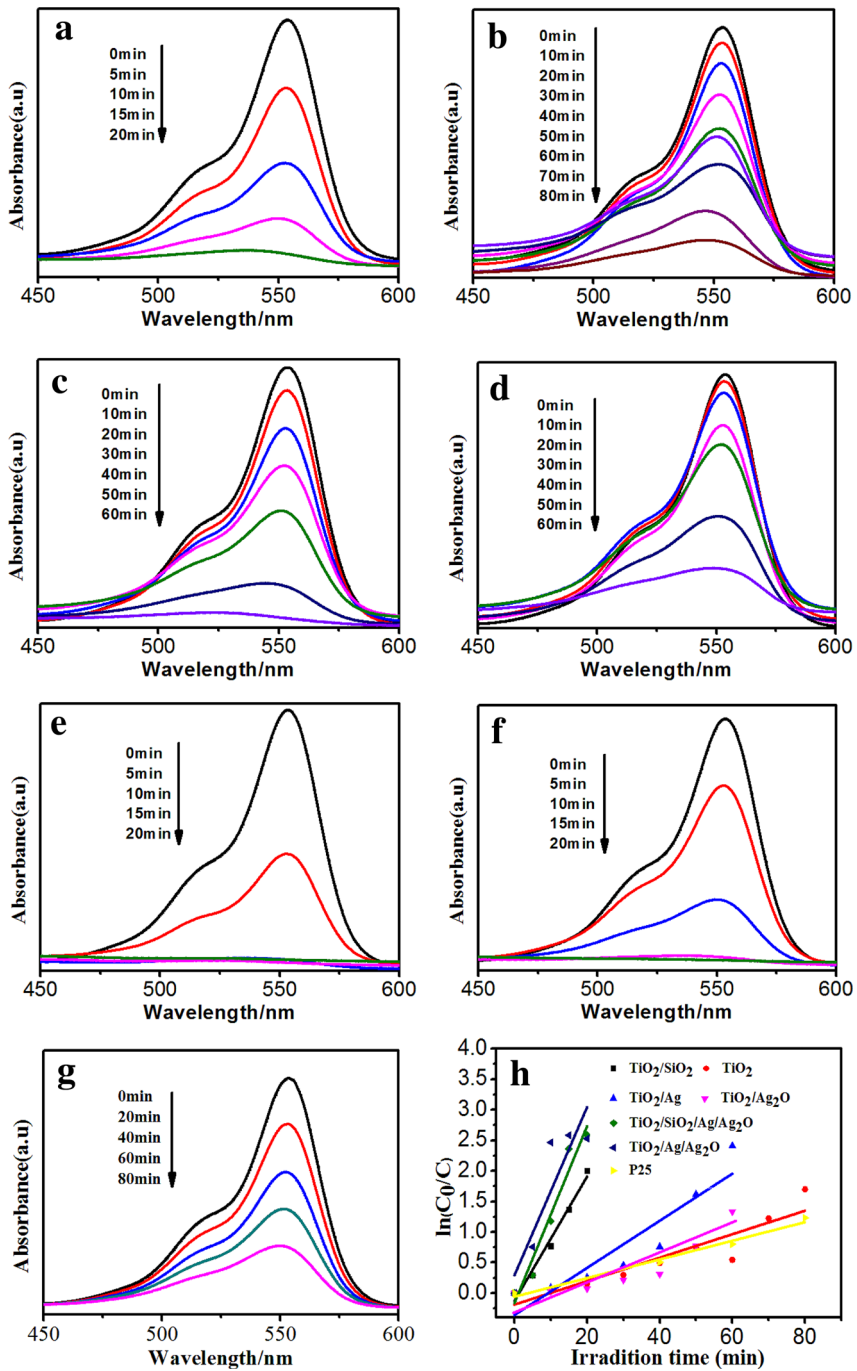


**Fig. 5** UV-Vis diffuse reflectance spectra (a) and estimated energy band gap (b) of the catalysts

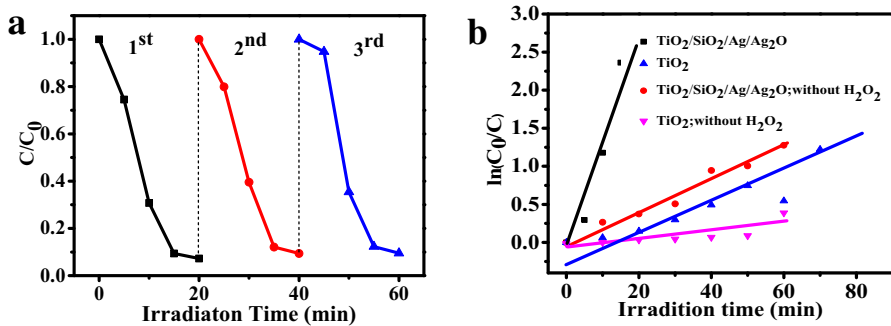
TiO<sub>2</sub> nanoparticles (P25) was also measured for comparison, and the results are displayed in Fig. 6. As can be seen from Fig. 6a, b, the absorbance of RhB solution in the presence of TiO<sub>2</sub>/SiO<sub>2</sub> nanocomposite spheres decreased more quickly compared with porous TiO<sub>2</sub> nanospheres, which indicates that TiO<sub>2</sub>/SiO<sub>2</sub> nanocomposite spheres have a relatively rapid degradation rate. That is to say, the silica core can contribute to improving the photocatalytic performance of TiO<sub>2</sub>. When porous TiO<sub>2</sub> nanospheres were modified by Ag or Ag<sub>2</sub>O, the degradation rate of RhB was improved (Fig. 6c, d), and when Ag and Ag<sub>2</sub>O NPs were deposited on the surface of porous TiO<sub>2</sub> nanospheres and TiO<sub>2</sub>/SiO<sub>2</sub> nanocomposite spheres, the photocatalytic efficiencies of the nanocomposite spheres were remarkably enhanced due to the synergistic effect of Ag and Ag<sub>2</sub>O. As shown in Fig. 6e–g, the degradation of RhB could be completed within 20 min, while the degradation efficiency of P25 was very low. Based on the above, it can be concluded that TiO<sub>2</sub>/Ag/Ag<sub>2</sub>O and TiO<sub>2</sub>/SiO<sub>2</sub>/Ag/Ag<sub>2</sub>O nanocomposite spheres exhibit superior photocatalytic abilities.

Figure 6h indicates the degradation kinetics of RhB fitted by using the equation  $kt = \ln(C_0/C)$ , in which  $k$ ,  $C_0$  and  $C$  represent the slope of the straight line, and the concentration of RhB after illumination for 0 min and  $t$  min, respectively [46]. The photocatalytic activities of the catalysts can be clearly observed by comparing the slope of the lines shown in Fig. 6h. The order of the photocatalytic activity of the obtained sphere structures is as follows, TiO<sub>2</sub>/SiO<sub>2</sub>/Ag/Ag<sub>2</sub>O ( $k = 0.145$ ) > TiO<sub>2</sub>/Ag/Ag<sub>2</sub>O ( $k = 0.138$ ) > TiO<sub>2</sub>/SiO<sub>2</sub> ( $k = 0.102$ ) > TiO<sub>2</sub>/Ag ( $k = 0.039$ ) > TiO<sub>2</sub>/Ag<sub>2</sub>O ( $k = 0.020$ ) > TiO<sub>2</sub> ( $k = 0.019$ ) > P25 ( $k = 0.015$ ). These results reveal that all the TiO<sub>2</sub> nanocomposite spheres show better photocatalytic efficiencies than porous TiO<sub>2</sub> nanospheres and P25, and TiO<sub>2</sub>/SiO<sub>2</sub>/Ag/Ag<sub>2</sub>O and TiO<sub>2</sub>/Ag/Ag<sub>2</sub>O nanocomposite spheres exhibit excellent photocatalytic performances.

The recycling efficiency of catalysts has a great influence on its further application. Therefore, it is necessary to carry out the cyclic experiment of the photocatalytic degradation of RhB solution. As illustrated in Fig. 7a, after three cycles of degradation of the RhB solution, TiO<sub>2</sub>/SiO<sub>2</sub>/Ag/Ag<sub>2</sub>O nanocomposite



**Fig. 6** UV-visible absorption spectra of **a**  $\text{TiO}_2/\text{SiO}_2$ , **b** porous  $\text{TiO}_2$  nanospheres, **c**  $\text{TiO}_2/\text{Ag}$ , **d**  $\text{TiO}_2/\text{Ag}_2\text{O}$ , **e**  $\text{TiO}_2/\text{Ag}/\text{Ag}_2\text{O}$ , **f**  $\text{TiO}_2/\text{SiO}_2/\text{Ag}/\text{Ag}_2\text{O}$  and **g** P25. **h** The corresponding degradation kinetics of RhB



**Fig. 7** **a** Cyclic degradation efficiency of TiO<sub>2</sub>/SiO<sub>2</sub>/Ag/Ag<sub>2</sub>O nanocomposite spheres under simulated solar irradiation; **b** the effect of H<sub>2</sub>O<sub>2</sub> addition on the degradation efficiency of TiO<sub>2</sub>/SiO<sub>2</sub>/Ag/Ag<sub>2</sub>O nanocomposite spheres and porous TiO<sub>2</sub> nanospheres

spheres still possess good photocatalytic activity, revealing that the prepared catalysts have excellent stability and ideal catalytic longevity.

As a commonly used co-catalyst, H<sub>2</sub>O<sub>2</sub> can improve the degradation performance of the catalysts and shorten the catalytic reaction time. The intrinsic effect of H<sub>2</sub>O<sub>2</sub> on the photocatalytic performance has also been investigated. Figure 7b shows the degradation kinetics of RhB over TiO<sub>2</sub>/SiO<sub>2</sub>/Ag/Ag<sub>2</sub>O nanocomposite spheres and porous TiO<sub>2</sub> nanospheres without H<sub>2</sub>O<sub>2</sub>. As shown in Fig. 7b, the degradation properties of TiO<sub>2</sub>/SiO<sub>2</sub>/Ag/Ag<sub>2</sub>O nanocomposite spheres and porous TiO<sub>2</sub> nanospheres are significantly improved after adding H<sub>2</sub>O<sub>2</sub>. This may be due to an inhibition of photoelectron–hole recombination and the generation of OH radicals caused by adding H<sub>2</sub>O<sub>2</sub> under simulated solar irradiation. In addition, the photocatalytic activity of TiO<sub>2</sub>/SiO<sub>2</sub>/Ag/Ag<sub>2</sub>O nanocomposite spheres is superior to porous TiO<sub>2</sub> nanospheres regardless of whether or not H<sub>2</sub>O<sub>2</sub> was added to the solution.

### Mechanism of photocatalytic activity

In order to explore the internal reasons for the excellent photocatalytic performance of TiO<sub>2</sub>/SiO<sub>2</sub>/Ag/Ag<sub>2</sub>O nanocomposite spheres, the illustration of the RhB degradation mechanism over the prepared catalysts under simulated solar irradiation is depicted in Fig. 8a. Since the silica core can provide a larger specific surface and more surface active sites for TiO<sub>2</sub>, this kind of structure has excellent adsorption properties for positively charged RhB in solution. Under simulated solar irradiation, Ag is first activated by the visible light and produces photoelectron–hole pairs because of the SPR effect [47]. And then, the photoelectrons (e<sup>-</sup>) on the surface of Ag shift rapidly to the conduction band (CB) of TiO<sub>2</sub> and Ag<sub>2</sub>O. Moreover, the excited electrons at the CB of Ag<sub>2</sub>O transfer to the CB of TiO<sub>2</sub> while the holes (h<sup>+</sup>) at the valence band (VB) of TiO<sub>2</sub> move to the VB of Ag<sub>2</sub>O, achieving the separation of photoelectron–hole pairs. The photo-generated electrons and holes can react with O<sub>2</sub> and H<sub>2</sub>O adsorbed on the surface of the catalysts to form O<sub>2</sub><sup>-</sup> and OH<sup>·</sup>, respectively [48]. In addition, a portion of the photoelectrons of TiO<sub>2</sub> and Ag<sub>2</sub>O are

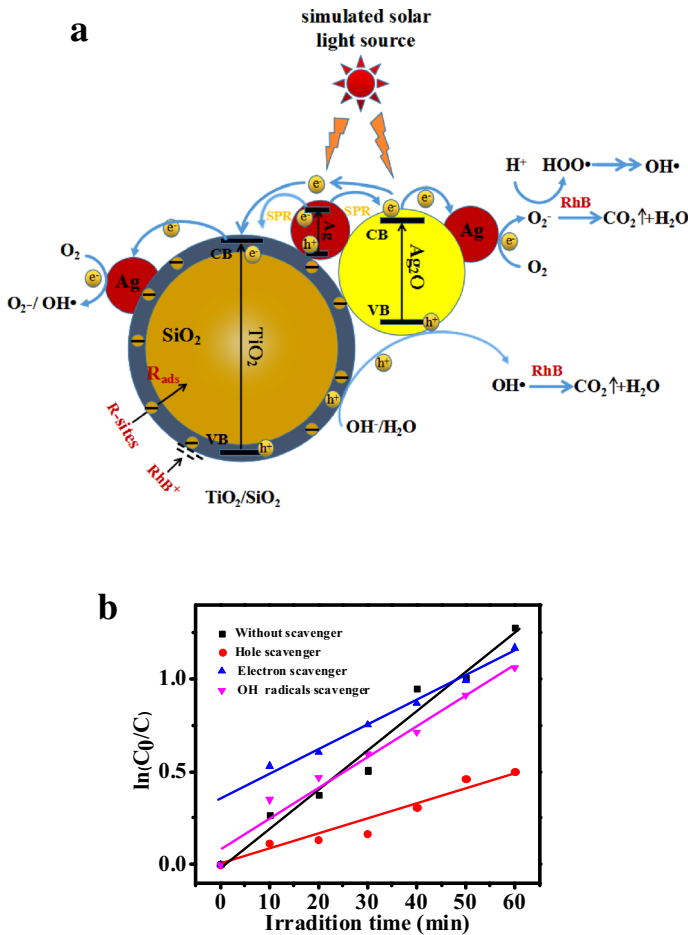


**Fig. 8** RhB degradation mechanism (a) and the effect of various scavengers on the degradation efficiency (b) of  $\text{TiO}_2/\text{SiO}_2/\text{Ag}/\text{Ag}_2\text{O}$  nanocomposite spheres under simulated solar irradiation

also quickly captured by the dissolved  $\text{O}_2$  on the surface of Ag and generate  $\text{O}_2^-$  and  $\text{OH}^\bullet$ . All of the above active radical species ( $\text{O}_2^-$ ,  $\text{OH}^\bullet$ ) can efficiently decompose the RhB adsorbed on the surface of  $\text{TiO}_2/\text{SiO}_2/\text{Ag}/\text{Ag}_2\text{O}$  nanocomposite spheres. Various scavengers were used to determine the main active species in the process of photocatalytic degradation. Figure 8b presents the effect of different scavengers on the degradation efficiency of  $\text{TiO}_2/\text{SiO}_2/\text{Ag}/\text{Ag}_2\text{O}$  nanocomposite spheres. The sequence of their degradation activities is as follows: no scavenger ( $k = 0.021$ ) > OH radicals ( $k = 0.0177$ ) > electron ( $k = 0.0167$ ) > hole ( $k = 0.008$ ). Obviously, the presence of scavengers inhibits the degradation of RhB. This indicates that holes, electrons and OH radicals play an important role in the degradation process. The trapping of holes ( $\text{h}^+$ ) leads to an inferior degradation performance, i.e., the holes are the main active species in the photocatalytic degradation of RhB. Therefore, the  $\text{TiO}_2/\text{SiO}_2/\text{Ag}/\text{Ag}_2\text{O}$  nanocomposite spheres

have an excellent photocatalytic degradation performance owing to the synergistic effects of different kinds of nanoparticles.

## Conclusions

In summary, a novel synthetic method was used to prepare  $\text{TiO}_2/\text{SiO}_2/\text{Ag}/\text{Ag}_2\text{O}$  and  $\text{TiO}_2/\text{Ag}/\text{Ag}_2\text{O}$  nanocomposite spheres. Both Ag and  $\text{Ag}_2\text{O}$  NPs were formed on  $\text{TiO}_2/\text{SiO}_2$  nanocomposite spheres or porous  $\text{TiO}_2$  nanospheres. The formed nanoheterojunctions can possess large specific surface areas, wide spectral responses and low photoelectron–hole recombination rates. The photocatalytic experiments indicate that all the prepared  $\text{TiO}_2$  nanocomposite spheres, especially  $\text{TiO}_2/\text{SiO}_2/\text{Ag}/\text{Ag}_2\text{O}$  and  $\text{TiO}_2/\text{Ag}/\text{Ag}_2\text{O}$ , exhibit superior photocatalytic efficiencies in comparison with porous  $\text{TiO}_2$  nanospheres and P25. Therefore, the obtained catalysts should have a potential application in sewage treatment. This study also strongly confirmed that the synergistic effects between different kinds of nanoparticles (Ag,  $\text{Ag}_2\text{O}$ ,  $\text{TiO}_2$  and  $\text{SiO}_2$ ) play a decisive role in affecting the photocatalytic performances of the synthesized nanocomposites.

**Acknowledgements** This work was supported by the National Natural Science Foundation of China (Grant No. 61774070), the Natural Science Foundation of Jiangsu Province (Grant No. BK20161300), the Six Talent Peaks Project in Jiangsu Province (Grant No. XNY-008), and also sponsored by Qing Lan Project and 333 Project of Jiangsu Province.

## References

1. Y.C. Yao, X.R. Dai, X.Y. Hu, S.Z. Huang, Z. Jin, *Appl. Surf. Sci.* **387**, 469 (2016)
2. S.B. Bai, K.Z. Zhang, J.H. Sun, R.X. Luo, D.Q. Li, A.F. Chen, *CrystEngComm* **16**, 3289 (2014)
3. X.H. Huang, M. Leal, Q.L. Li, *Water Res.* **42**, 1142 (2008)
4. H.J. Zhang, G.D. Du, W.Q. Lu, L.L. Cheng, X.D. Zhu, Z. Jiao, *CrystEngComm* **14**, 3793 (2012)
5. Z.F. Wang, D.Q. Chu, L.M. Wang, L.P. Wang, W.H. Hu, *Appl. Surf. Sci.* **396**, 492 (2017)
6. A.P. Batista, H.W.P. Carvalho, G.H. Luz, P.F. Martins, M. Gonçalves, L.C. Oliveira, *Environ. Chem. Lett.* **8**, 63 (2010)
7. X.F. Wang, S.F. Li, H.G. Yu, J.G. Yu, S.W. Liu, *Chem. Eur. J.* **17**, 7777 (2011)
8. S. Chakrabarti, B.K. Dutta, *J. Hazard. Mater.* **112**, 269 (2004)
9. Y.N. Tan, C.L. Wong, A.R. Mohamed, *ISRN Mater. Sci.* **2011**, 1 (2011)
10. Z.H. Zhang, Y. Xu, X.P. Ma, F.Y. Li, D.N. Liu, Z.L. Chen, F.Q. Zhang, D.D. Dionysiou, *J. Hazard. Mater.* **209**, 271 (2012)
11. H.G. Yang, G. Liu, S.Z. Qiao, C.H. Sun, Y.G. Jin, S.C. Smith, *J. Am. Chem. Soc.* **13**, 4078 (2009)
12. Z.Q. Li, Y. Ding, L.E. Mo, L.H. Hu, J.H. Wu, S.Y. Dai, *ACS. Appl. Mater. Interfaces* **7**, 22277 (2015)
13. X. Chen, S.S. Mao, *Chem. Rev.* **107**, 2891 (2007)
14. J.R. Huang, H.B. Ren, X.S. Liu, X.X. Li, J.J. Shim, *Superlattices Microstruct.* **81**, 16 (2015)
15. T.V. Gerasimova, O.L. Evdokimova, A.S. Kraev, V.K. Lvanov, A.V. Agafonov, *Microporous Mesoporous Mater.* **235**, 185 (2016)
16. K.C. Christoforidis, A. Sengele, V. Keller, N. Keller, *ACS. Appl. Mater. Interfaces* **7**, 19324 (2015)
17. Y. Qiu, L.P. Wu, J. Li, X.J. Li, *Catal. Lett.* **145**, 647 (2015)
18. L.J. Alemany, M.A. Ban, E. Pardo, F. Martin, M. Galan-Fereres, J. Blasco, *Appl. Catal. B Environ.* **3**, 289 (1997)
19. W.H. Dong, F.P. Pan, L.L. Xu, M.R. Zheng, C.H. Sow, K. Wu, *Appl. Surf. Sci.* **349**, 279 (2015)
20. S.Q. Liu, N.Z. Zhang, Z.R. Tang, Y.J. Xu, *ACS. Appl. Mater. Interfaces* **4**, 6378 (2012)



21. X.J. Liu, L.K. Pan, T. Lv, Z. Sun, C.Q. Sun, RSC Adv. **2**, 3823 (2012)
22. N.D. Feng, Q.W. Wang, A.M. Zheng, Z.F. Zhang, J. Fan, S.B. Liu, J. Am. Chem. Soc. **135**, 1607 (2013)
23. K. Lalitha, G. Sadanandam, V.D. Kumari, M. Subrahmanyam, B. Sreedhar, N.Y. Hebalkar, J. Phys. Chem. C **114**, 22181 (2010)
24. G.H. Li, N.M. Dimitrijevic, L. Chen, T. Rajh, K.A. Gray, J. Phys. Chem. C **112**, 19040 (2008)
25. L.M. Lyu, M.H. Huang, J. Phys. Chem. C **115**, 17768 (2011)
26. D. Sarkar, C.K. Ghosh, S. Mukherjee, K.K. Chattopadhyay, ACS Appl. Mater. Interfaces **5**, 331 (2013)
27. X.K. Tang, Q.M. Feng, K. Liu, Y. Tan, Mater. Lett. **183**, 175 (2016)
28. K. Liu, Q.M. Feng, Y.X. Yang, G.F. Zhang, L.M. Ou, Y.P. Lu, J. Non-Cryst. Solids **353**, 1534 (2007)
29. M.M. Ye, H.H. Zhou, T.Q. Zhang, Y.P. Zhang, Y. Shao, Chem. Eng. J. **226**, 209 (2013)
30. Y. Ren, M. Chen, Y. Zhang, L.M. Wu, Langmuir **26**, 11391 (2010)
31. M. Bellardita, M. Addamo, A. Di Paola, G. Marci, L. Palmisano, J. Hazard. Mater. **174**, 707 (2010)
32. Z.H. Li, J.W. Liu, D.J. Wang, Y. Gao, J. Shen, Int. J. Hydrog. Energy **37**, 6431 (2012)
33. N.D. Feng, A.M. Zheng, Q. Wang, P.P. Ren, X.Z. Gao, S.B. Liu, J. Phys. Chem. C **115**, 2709 (2011)
34. C.B. Liu, C.H. Cao, X.B. Luo, S.L. Luo, J. Hazard. Mater. **285**, 319 (2015)
35. T.A. Gad-Allah, S. Kato, S. Satokawa, T. Kojima, Desalination **244**, 1 (2009)
36. Y. Chi, Q. Yuan, Y.J. Li, L. Zhao, N. Li, X.T. Li, W.F. Yan, J. Hazard. Mater. **262**, 404 (2013)
37. S.A. Khan, S. Ali, M. Sohail, M.A. Morsy, Z.H. Yamani, Aust. J. Chem. **69**, 41 (2016)
38. S.P. Prakoso, A. Taufik, R. Saleh, IOP Conf. Ser. Mater. Sci. Eng. **188**, 012029 (2017)
39. Y.Q. Cui, Q.L. Ma, X.Y. Deng, Q. Meng, X.W. Cheng, M.Z. Xie, Appl. Catal. B: Environ. **206**, 136 (2017)
40. D. He, S. Garg, T.D. Waite, Langmuir **28**, 10266 (2012)
41. B. Jiang, L.L. Jiang, X.W. Shi, W.C. Wang, G.S. Li, F.X. Zhu, D.Q. Zhang, J. Sol-Gel, Sci. Technol. **73**, 314 (2015)
42. S.Q. Liu, N. Zhang, Z.R. Tang, Y.J. Xu, ACS Appl. Mater. Interfaces **4**, 6378 (2012)
43. Z.Q. Cheng, S.Z. Zhao, Z.L. Han, Y.Q. Zhang, X.D. Zhao, L.J. Kang, CrystEngComm **18**, 8756 (2016)
44. W.J. Zhou, H. Liu, J.Y. Wang, D. Liu, G.J. Du, J.J. Cui, ACS Appl. Mater. Interfaces **2**, 2385 (2010)
45. S. Liu, N. Wang, Y. Zhang, J. Hazard. Mater. **284**, 171 (2015)
46. Z. Zhu, Y. Yan, J. Li, J. Mater. Sci. **51**, 2112 (2016)
47. C. Liu, D. Yang, Y. Jiao, Y. Tian, Y.G. Wang, Z.Y. Jiang, ACS Appl. Mater. Interfaces **5**, 3824 (2013)
48. S. Linic, P. Christopher, D.B. Ingram, Nat. Mater. **10**, 911 (2011)